The adsorption and desorption of ethanol ices from a model grain surface

Article (Published Version)

The adsorption and desorption of ethanol ices from a model grain surface

D. J. Burke, A. J. Wolff, J. L. Edridge, and W. A. Brown

Citation: The Journal of Chemical Physics **128**, 104702 (2008); doi: 10.1063/1.2888556
View online: http://dx.doi.org/10.1063/1.2888556
View Table of Contents: http://scitation.aip.org/content/aip/journal/jcp/128/10?ver=pdfcov
Published by the AIP Publishing

The adsorption and desorption of ethanol ices from a model grain surface

D. J. Burke, A. J. Wolff, J. L. Edridge, and W. A. Brown[a)]
Department of Chemistry, University College London, 20 Gordon Street, London WC1H 0AJ, United Kingdom

(Received 26 September 2007; accepted 4 February 2008; published online 12 March 2008)

Reflection absorption infrared spectroscopy (RAIRS) and temperature programed desorption (TPD) have been used to probe the adsorption and desorption of ethanol on highly ordered pyrolytic graphite (HOPG) at 98 K. RAIR spectra for ethanol show that it forms physisorbed multilayers on the surface at 98 K. Annealing multilayer ethanol ices (exposures >50 L) beyond 120 K gives rise to a change in morphology before crystallization within the ice occurs. TPD shows that ethanol adsorbs and desorbs molecularly on the HOPG surface and shows four different species in desorption. At low coverage, desorption of monolayer ethanol is observed and is described by first-order kinetics. With increasing coverage, a second TPD peak is observed at a lower temperature, which is assigned to an ethanol bilayer. When the coverage is further increased, a second multilayer, less strongly bound to the underlying ethanol ice film, is observed. This peak dominates the TPD spectra with increasing coverage and is characterized by fractional-order kinetics and a desorption energy of 56.3 ± 1.7 kJ mol^{-1}. At exposures exceeding 50 L, formation of crystalline ethanol is also observed as a high temperature shoulder on the TPD spectrum at 160 K. © *2008 American Institute of Physics*. [DOI: 10.1063/1.2888556]

I. INTRODUCTION

Ethanol has been detected in the interstellar medium (ISM) in both the gas and condensed phases in star forming regions known as hot cores.[1–3] The abundance of gas-phase ethanol in these regions has been estimated to lie in the region of 10^{-6}–10^{-8} relative to molecular hydrogen.[2,4] However, even the lowest abundances of gas-phase ethanol cannot be reproduced by gas-phase chemistry models.[5,6] The origin of these enhanced gas-phase abundances is thought to arise from the evaporation of interstellar ices that have frozen out on the surface of dust grains.[1,7] Once released into the gas phase, ethanol has been predicted to drive the formation of complex organic molecules such as dimethyl ether.[8]

It has been well documented that interstellar dust grains play a pivotal role in chemical and molecular evolutionary processes in the ISM.[2,9] These carbonaceous and silicaceous particles open up reaction pathways to molecules/atoms that readily accrete on the grains, which are not available in the gas phase. The interstellar ices that are formed on dust grains are dominated by H_2O, CH_3OH, and CO,[10] with ethanol composition within these ices estimated to lie between 0.5% and 5% relative to H_2O.[8] However, Infrared Space Observatory (ISO) data suggest the upper limit of solid ethanol to be 1.2% within these ices.[11]

Several surface-mediated mechanisms have been proposed to account for the formation of ethanol via grain surface chemistry.[8,12,13] Tunneling reactions, leading to the formation of ethanol via the successive hydrogenation of acetylene, followed by oxidation of the resulting ethyl radical have been suggested.[8,12] Alternatively, radical-radical reactions within bulk molecular ices have also been proposed. Temperatures in the region of hot cores lead to the annealing of interstellar ices, giving rise to radical diffusion. Subsequent reactions between methyl, ethyl, and hydroxyl radicals may lead to the formation of simple alcohols.[8] More recently, Shriver *et al.* performed irradiation experiments on CO_2/C_2H_6 matrices.[13] The detection of ethanol in infrared (IR) spectra after irradiation was ascribed to the formation of hot atomic oxygen from the photodissociation of CO_2, which in turn inserted itself into the C–H bond of a C_2H_6 molecule. However, despite these hypotheses, the exact nature of ethanol formation on dust grain surfaces still remains unclear.

In order to begin to elucidate possible surface reaction pathways, a detailed characterization of the fundamental surface interactions of ethanol adsorbed on interstellar dust grains needs to be established. Hence, in this paper, we report a detailed investigation of the adsorption and desorption of ethanol on a model dust grain surface. More specifically, reflection absorption infrared spectroscopy (RAIRS) and temperature programed desorption (TPD) have been used to probe ethanol adsorption and desorption from a highly ordered pyrolytic graphite (HOPG) surface held at 98 K. Dust grains in the ISM are thought to consist of carbonaceous and silicate materials; hence, HOPG can be considered a suitable dust grain analog.

There have been a number of IR spectroscopic studies of the various phases of ethanol and its deuterated counterparts reported in the literature.[11,14–20] A detailed study by Perchard and Josien[14,15] examined gas, diluted solution, liquid, and solid state phases of ethanol, reporting 19 different vibrational bands. Assignment was made difficult based on coupling between the vibrational modes observed in each phase. Barnes and Hallam measured the IR spectra of ethanol suspended in argon matrices at 20 K.[17]

[a)]Author to whom correspondence should be addressed. Electronic mail: w.a.brown@ucl.ac.uk.

The small bandwidths in the low temperature matrix allowed bands arising from the two conformers of the ethanol molecule to be resolved and, as a consequence, proposed alternative assignments to those made by Perchard and Josien. More recently, Coussan *et al.*[18] have measured the vibrational spectrum of ethanol trapped in both argon and nitrogen matrices at 9 K. Experimental data, used in conjunction with *ab initio* calculations, showed that only one form of ethanol conformer was stabilized within the argon matrix and this was insensitive to thermal cycling up to 30 K. Additional studies have measured IR spectra of single crystal ethanol and ethanol in the liquid phase.[16]

A limited number of IR studies of multilayer ethanol ices adsorbed on surfaces have been performed.[11,19,21] Camplin and McCash performed a RAIRS study of methanol and ethanol on an oxygen covered Cu(100) surface at 78 K.[19] Spectra of physisorbed ethanol ices, in addition to four deuterated analogs, were presented. Vibrational assignments of the observed IR modes were in good agreement with those reported for matrix isolation data[17] and the gas, liquid, and glass states.[14,15] Similarly, Eng *et al.* in their investigation of multilayer ethanol on Si(100) at 135 K (Ref. 21) were able to assign vibrational bands based on the measurements of Perchard and Josien, proposing alternative assignments based on their *ab initio* calculations. From an astronomical perspective, Boudin *et al.* undertook a study of six different species, including ethanol, that are considered to be important constituents of interstellar ices and comets.[11] IR spectroscopic data of pure ethanol films were recorded on a CsI substrate at 10 K, in addition to ethanol embedded in both H_2O and CO dominated ices.

On transition metal surfaces, ethanol has been the subject of numerous studies,[19,22–30] mainly due to the potential of ethanol as an alternative fuel source. Studies have been conducted on Pt,[22–24] Cu,[19,25] Rh,[26,27] Pd,[28] Ni,[29] and Ir (Ref. 30) single crystal surfaces. Ethanol is observed to adsorb molecularly at low temperature[22–24,26,28–30] bonding to the substrate via the O atom[24,26] (or both O and H moieties[29]) with the O–H bond almost parallel to the surface. Desorption channels and decomposition pathways are dependent on the metal surface. Panja *et al.* observed that the entire ethanol monolayer desorbed reversibly on Pt(111).[22] However, the more general trend is that ethanol dissociates on transition metal surfaces upon heating.

On HOPG, there have been only a limited number of previous studies of ethanol adsorption, with a few authors reporting energies of desorption for monolayer and multilayer coverages.[31,32] Ulbricht *et al.*[32] performed a study of numerous adsorbates on both the basal plane of HOPG and single-walled carbon nanotube samples. Ethanol was included in the investigation and they reported desorption energies of 50 ± 3 and 46 ± 3 kJ mol^{-1} for the monolayer and multilayer (4 ML), respectively. Desorption kinetics for a series of fluorinated ethers and alcohols adsorbed on the basal plane of graphite at temperatures <90 K were determined by Shukla *et al.*[31] These results were compared to hydrocarbon analogs. Desorption energies of 57.6 ± 0.7 kJ mol^{-1} for the monolayer and 46.4 ± 0.8 kJ mol^{-1} for 2 ML were obtained. X-ray diffraction measurements of monolayer ethanol adsorbed on exfoliated graphite between 30 and 215 K were performed by Morishige.[33] It was determined that crystalline monolayer ethanol adsorbed on the surface with zigzag chains of hydrogen bonds, with molecules closely packing together in two dimensions. These results were in agreement with previous neutron diffraction measurements.[34]

In the following, we present a detailed RAIRS and TPD investigation of ethanol adsorption on and desorption from HOPG at 98 K. All measurements are reported as a function of surface exposure, ranging from 0.5 to 300 L. The experiments in this study are performed at temperatures that are slightly higher when compared to those measured in the ISM (10–20 K). However, temperatures in the region of hot cores typically range between 100 and 300 K,[35] and it is within this temperature regime, as illustrated by the data in this study and others,[36–38] that the evaporation of molecular ices from dust grains occurs.

II. EXPERIMENTAL

Experiments were performed in a stainless steel ultrahigh vacuum (UHV) chamber. The background pressure in the chamber was better than 2×10^{-10} mbar. The HOPG sample was purchased from Goodfellows Ltd. and was cleaved prior to installation in the UHV chamber using the "Scotch tape" method.[39] The sample was mounted on the end of a liquid nitrogen cooled cold finger and the temperature was monitored with an *N*-type thermocouple. The base temperature of the assembly in these experiments was 98 K. The sample was cleaned before each experiment by annealing at 500 K in UHV for 3 min. Sample cleanliness was confirmed by the absence of any desorption during TPD experiments performed with no dosage. Ethanol (99.7%–100%, AnalaR BDH) was purified by repeated freeze-pump-thaw cycles. Ethanol ices were grown *in situ* by backfilling the chamber through a high precision leak valve. All exposures are measured in langmuir, where 1 L$=10^{-6}$ mbar s. RAIR spectra were recorded using a Mattson Instruments RSI Research Series Fourier transform IR spectrometer coupled to a liquid nitrogen cooled mercury cadmium telluride detector. All spectra were taken at a resolution of 4 cm^{-1} and are the result of the coaddition of 256 scans. For the annealed RAIRS experiments, the sample temperature was raised and held at a predetermined temperature for 3 min before cooling back to the base temperature where a spectrum was recorded. TPD spectra were recorded with a Hiden Analytical HAL201 quadrupole mass spectrometer. All TPD spectra were recorded at a heating rate of 0.50 ± 0.01 K s^{-1}.

III. RESULTS AND DISCUSSION

A. RAIRS data

1. Adsorption

RAIR spectra following the adsorption of ethanol on HOPG at 98 K are shown in Fig. 1. At the lowest exposure (5 L), six peaks appear in the spectrum at 2972, 2896, 1380, 1095, 1057, and 887 cm^{-1}. Increasing the exposure to 10 L sees the appearance of two new bands: A very broad band

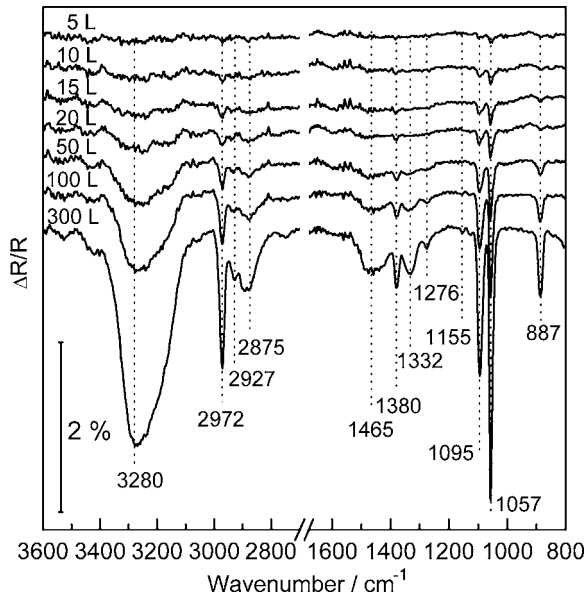

FIG. 1. RAIR spectra for increasing exposures of ethanol on HOPG at 98 K. Exposures are shown in the figure. The region between 1700 and 2700 cm^{-1}, which exhibits no vibrational bands, has been omitted for clarity.

centered at 3280 cm^{-1} and a low intensity band at 2875 cm^{-1}. Successive increases in dose reveal the presence of four new features: A band at 2927 cm^{-1} appears at 15 L, two new bands at 1276 and 1332 cm^{-1} are seen at 50 L, and a very broad band appears at 20 L centered around 1460 cm^{-1}. The latter retains its complexity up to an exposure of 300 L, comprising a collection of peaks at 1488, 1475, 1457, and 1438 cm^{-1}. No further bands are observed until a low intensity band grows into the spectrum at an exposure of 300 L, located at 1155 cm^{-1}.

Once the bands described above have grown into the spectrum, increasing the ethanol exposure up to 300 L sees a corresponding increase in intensity of all bands with no associated spectral shift. Furthermore, none of the bands saturate with increasing coverage. These observations indicate that both monolayer and multilayer forms of ethanol, which are clearly distinguished in the TPD data (see later), are physisorbed on the surface of HOPG at 98 K.

Assignments of the observed IR bands have been made with reference to previous work of ethanol adsorption on other substrates[11,19,21] and within argon matrices.[17,18] In addition, IR bands in the gas phase, diluted solution, solid state, and liquid phase[14–16] have also been used to aid assignment. A full assignment of the vibrational bands seen in Fig. 1 is summarized in Table I. Assignment of the majority of the bands is straightforward, based on good agreement with previous data. However, there are some ambiguities with regard to specific bands, most notably the peaks observed within the low frequency region at 887, 1057, and 1095 cm^{-1}, in addition to the high frequency band at 3280 cm^{-1}. The low frequency bands have been assigned primarily by comparison with those of Boudin *et al.* who reported IR measurements of multilayer ethanol adsorbed on a CsI surface at 10 K.[11] The data obtained on the CsI surface were chosen based on the overall consistency of the peak positions across the entire spectrum compared to the data obtained in Fig. 1. The high frequency band at 3280 cm^{-1} has been assigned to the υ(OH) stretch. This peak is downshifted by approximately 400 cm^{-1} when compared to the same band assigned in the gas phase (3676 cm^{-1}) (Refs. 14 and 15) and within an Ar matrix (3658 cm^{-1}) (Ref. 18) but is in good agreement with that observed for ices grown on substrates and in the liquid

TABLE I. Assignment of the vibrational bands observed in the RAIR spectra of ethanol multilayers adsorbed on HOPG at 98 K. For comparison, the table includes IR band assignments for ethanol multilayers adsorbed on CsI, oxidized Cu(100), and Si(100) substrates, in addition to ethanol suspended in argon matrices and vitreous phase. Bands below 850 cm^{-1} have been omitted for clarity. Bands denoted by # were not observed in the related study.

Vibrational mode (cm^{-1})	Multilayer C_2H_5OH/HOPG (98 K)	Multilayer C_2H_5OH/CsI (10 K)[a]	Multilayer C_2H_5OH/oxidized Cu(100) (78 K)[b]	Multilayer C_2H_5OH/Si(100) (135 K)[c]	C_2H_5OH/Ar matrix (20 K)[d]	Vitreous C_2H_5OH (80 K)[e]
υ(CC)	887	879	882	891	887	881,886
υ(CO)	1057	1049	1058	1061	1025,1083	1051
ρ(CH_3)	1095	1089	1097	1099	1092	1091
ρ'(CH_3)	1155	1156	#	#	#	1128
τ(CH_2)	1276	1275	1277	#	1240,1251	1277
δ(OH)	1332	1329	1341	1335	#	1331
δ_s(CH_3)	1380	1381	1382	1385	1371	1381
ω(CH_2)	1438	1424	#	#	1415	#
δ_a(CH_3)	1457	1454	1457	1481	1445,1463	1410–1480
δ'_a(CH_3)	1475	1477	#	#	#	#
δ_s(CH_2)	1488	1487	#	#	1490	#
υ_s(CH_2)	2875,2896	2884	2874	2881	2901,2954	2873,2894
υ_s(CH_3)	2927	2930	2927	2928	2940	2928
υ_a(CH_3)	2972	2971	2974	2983	2996,2985	2970
υ(OH)	3280	3291	#	3267	3658	#

[a]Reference 11.
[b]Reference 19.
[c]Reference 21.
[d]Reference 17.
[e]References 14 and 15.

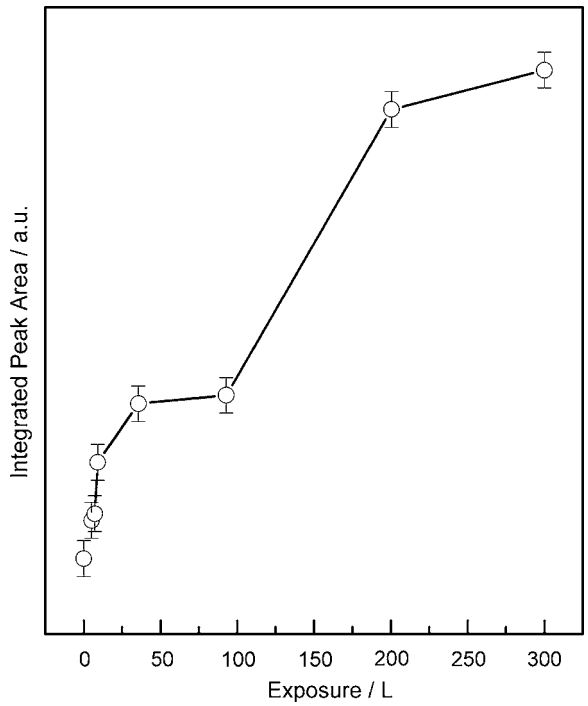

FIG. 2. A plot showing the integrated peak area of the entire spectral region between 3700 and 800 cm^{-1} as a function of ethanol exposure on HOPG at 98 K.

phase.[11,16,19,21] The downshift and broadness of this band are both characteristic of hydrogen bonded networks existing within the ethanol ice.

Figure 2 shows a plot of the integrated area of all vibrational bands observed in Fig. 1 over the entire spectral range as a function of dose. Exposures up to 20 L are characterized by a simple linear relationship. However, beyond this limit, the linearity breaks down. A linear uptake would typically indicate that the sticking probability remains constant over the entire exposure range, assuming that the molecular orientation remains unchanged as a function of exposure. Hence, the variation in the slope of the plot in Fig. 2 could indicate a change in the sticking probability of ethanol on the HOPG substrate compared to ethanol adsorption on an existing adlayer. This is not the case here, as the data in Fig. 2 are at odds with a similar calculation performed on the TPD data (see later), which in contrast exhibits a linear increase of relative surface coverage with increasing exposure. The different results for the RAIRS and TPD data can be explained by the dependence of the RAIR data (Fig. 2) on molecular orientation. In this case, the variation in the slope in Fig. 2 is probably due to a change in ethanol orientation for exposures above 20 L. The base temperature of the HOPG substrate (98 K) is very close to that of the glass transition temperature of amorphous ethanol (97 K) obtained from calorimetric studies.[40] This would suggest that upon adsorption, ethanol may form a viscous liquid phase on the HOPG surface. Hence, the ethanol molecule is sufficiently thermalized upon adsorption to permit a more energetically favorable bonding orientation on the surface. Since ethanol is physisorbed on the surface, the orientation will be dictated by lateral interactions between neighboring molecules rather than by interactions with the substrate.

RAIR spectra at low coverage permit some insight into the possible orientation of the first few layers adsorbed on the HOPG surface. The surface selection rules that apply to metal surfaces are also valid for the HOPG surface;[41] therefore, vibrational modes that contain a component of the dipole moment perpendicular to the surface are detected by RAIRS. At the lowest dose (5 L), six bands are visible, two assigned to the skeletal modes υ(CC) and υ(CO), and four assigned to the methyl modes $\rho(CH_3)$, $\delta_s(CH_3)$, $\upsilon_a(CH_3)$, and $\upsilon_s(CH_2)$. The prominence of these bands at low coverage suggests that within the first adlayer, the ethanol molecule has an upright configuration, with the CCO bonds lying in a plane perpendicular to the surface normal. The degree of freedom that is implied by the number of methyl bands observed at low coverage, in addition to the absence of the OH band, suggests that the OH group is closely associated with the HOPG surface. A similar ethanol molecular orientation

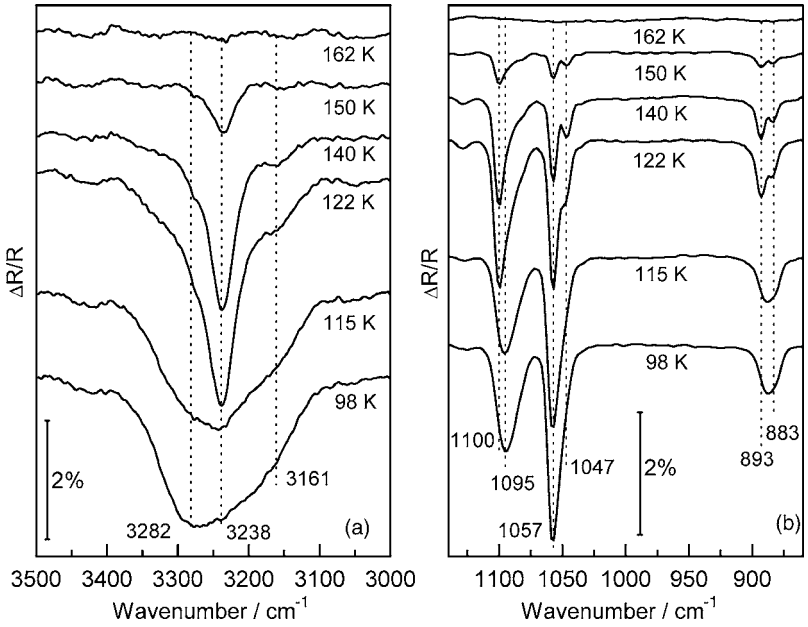

FIG. 3. RAIR spectra following successive annealing to increasing temperature of 300 L of ethanol adsorbed on HOPG at 98 K. (a) Region between 3500 and 3000 cm^{-1} illustrating the sharpening of the υ(OH) band. (b) Region between 1140 and 860 cm^{-1}, highlighting the υ(CC) and υ(CO) band splitting and the $\rho(CH_3)$ blueshift with increasing temperature.

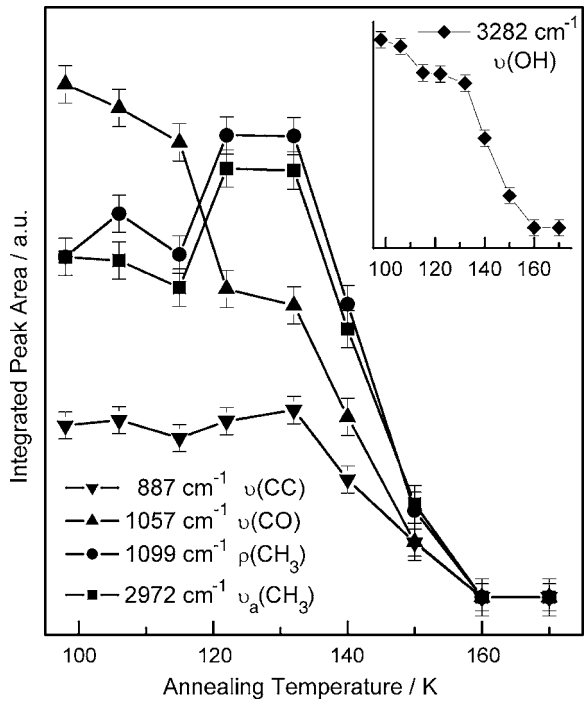

FIG. 4. A plot of the integrated area under selected vibrational bands as a function of annealing temperature. The inset shows the integrated area under the υ(OH) band as a function of annealing temperature.

within the first adlayer has been reported by Xu *et al.* who investigated ethanol adsorption on Ni(111) at 90 K.[29] Furthermore, Bolina *et al.* assigned a similar orientation to methanol physisorbed on HOPG at 97 K.[42]

2. Annealing the pure ethanol ice

The desorption behavior of the ethanol ices was investigated by performing a series of annealing experiments. In each case, the sample was elevated to the desired temperature, held for 3 min, and then recooled to 98 K prior to recording the RAIR spectrum. Three different thicknesses of ethanol films were studied: 300, 100, and 50 L. Annealing experiments performed with 100 and 50 L films exhibited similar behavior to that of the 300 L film, demonstrating that the effects observed are independent of exposure above 50 L. For clarity, the data for the 300 L ice will be used to illustrate the desorption and annealing trends.

Annealing to a temperature of 115 K does little to alter the spectral features, with only a minor change in the amplitude of some bands. However, annealing temperatures from 122 to 140 K see the onset of several changes across the spectrum, until desorption of the ethanol ice is complete at 162 K.

Figure 3(a) shows the effect of increasing the annealing temperature on the υ(OH) stretching region between 3500 and 3000 cm^{-1}. Figure 3(b) illustrates the region between 1140 and 860 cm^{-1}. At an annealing temperature of 122 K, the broad υ(OH) band at 3280 cm^{-1} begins to evolve into a sharp peak with an increased peak height at 3238 cm^{-1} and a low frequency shoulder at 3161 cm^{-1}. By 140 K, the sharp peak and low frequency shoulder have decreased in amplitude but exhibit sharper definition; this is coupled with the development of a high frequency shoulder at 3282 cm^{-1}. A continued decrease of intensity is observed until desorption is complete at 162 K.

RAIR spectra for the low frequency region are shown in Fig. 3(b). An annealing temperature of 122 K results in a blueshift of 5 cm^{-1} of the $\rho(CH_3)$ band from 1095 to 1100 cm^{-1}, coupled with an increase in amplitude. There is no further spectral shift in this peak with increasing temperature. The bands assigned to the skeletal modes, υ(CO) and υ(CC), exhibit a decrease in amplitude on heating to 115 K, before splitting at an annealing temperature of 122 K. The υ(CO) band develops a low frequency shoulder at 1047 cm^{-1} while retaining the 1057 cm^{-1} band. In contrast, the symmetric υ(CC) band evolves into two bands at 893 and 883 cm^{-1}. In each case, the new bands do not exhibit any further spectral shifts until complete desorption at 162 K. A similar trend is also observed for the two bands in the high frequency region, at 2972 and 2927 cm^{-1}, assigned to the asymmetric and symmetric methyl stretches, respectively, which exhibit an increase in amplitude at 122 K, with evidence of splitting around 140 K.

To examine the effects of annealing the ethanol ice further, the integrated areas of the five most dominant bands in the RAIR spectra as a function of annealing temperature were determined. The data are shown in Fig. 4, with the inset to Fig. 4 showing the υ(OH) vibration which is displayed on a larger scale. It is clear from Fig. 4 that the splitting and increase in band amplitudes observed for temperatures $>$122 K are a result of the onset of reordering of the ethanol molecules within the multilayer, rather than the consequence of desorption. Souda, using time-of-flight secondary ion mass spectrometry to investigate the interaction between amorphous ethanol and heavy water films on Ni(111), noted that a morphology change occurred within an ethanol multilayer at 120 K (Ref. 43) due to an increased film fluidity. The onset of the band changes in the RAIR data in this study evolve between 115 and 122 K, in good agreement with Souda's observation, and point to a similar change in film morphology.

The process of reorganization within the ethanol multilayers observed during the annealing process between 120 and 140 K can be attributed to the formation of crystalline ethanol within the multilayer film. Ayotte *et al.* reported a sharpening of the υ(OH) stretching region in the IR spectrum of nanoscale amorphous films of ethanol adsorbed on Pt(111).[44] The emergence of a narrow peak arising from the initial broad υ(OH) band at an annealing temperature of 135 K was ascribed to the formation of a fully crystallized film. In the same study, a similar effect was observed during the annealing of methanol films to 116 K. Furthermore, similar splitting of the υ(OH) band has been observed for physisorbed multilayers of methanol adsorbed on HOPG which was also ascribed to crystallization.[42] Figure 3(a) clearly exhibits this sharpening. However, the exact extent of crystallization within the ethanol films cannot be determined by RAIR spectra.

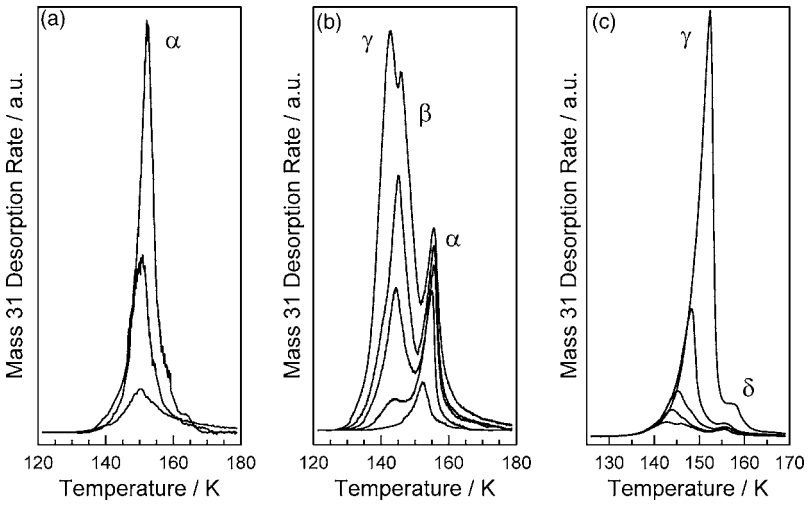

FIG. 5. Mass 31 TPD data for increasing exposures of ethanol on HOPG at 98 K. (a) Exposures of 0.5, 1, and 2 L showing the monolayer (α). (b) Exposures of 2, 5, 10, 15, and 25 L showing the monolayer (α), bilayer (β), and multilayer (γ) desorption peaks. (c) Exposures of 25, 35, 50, 100, and 300 L illustrating the formation of crystalline ethanol (δ) at ethanol exposures $\geqslant$50 L.

B. TPD data

1. Results

Figure 5 shows the mass 31 TPD data for a HOPG surface exposed to increasing amounts of ethanol at 98 K. The mass 31 ion is the major mass spectrometer cracking fragment of ethanol. To ensure that the fragment was not a result of any surface chemistry, experiments were performed that simultaneously monitored masses 46, 32, and 31. These exhibited identical ratios throughout, hence confirming that ethanol adsorbs reversibly on HOPG at 98 K.

At the lowest exposures shown in Fig. 5(a) (0.5–2 L), a single peak is observed in the TPD spectrum at ~151 K, denoted α. This peak increases in intensity and seemingly saturates at an exposure around 10 L [Fig. 5(b)]. Peak α is assigned to the desorption of monolayer ethanol physisorbed on the HOPG surface. It is the first to appear in the TPD spectrum and therefore must be ethanol that is directly associated with the surface. Closer inspection of the monolayer peak in Figs. 5(a) and 5(b) shows that the leading edges of the TPD traces are not shared. Furthermore, this peak exhibits an almost constant peak temperature over a large exposure range (0.5–35 L). These observations suggest that the monolayer desorbs with first-order kinetics, as confirmed later in Sec. III B 2.

Increasing the exposure from 5 to 15 L sees the successive appearance of two additional peaks, labeled β and γ, both of which are assigned to multilayer desorption. The feature labeled β appears in the spectrum at 5 L as a low temperature shoulder on the monolayer peak at 144 K, prior to the completion of the monolayer. This peak couples an increase of intensity with a minor upward shift of peak temperature and is clearly visible up to a dose of 25 L at a temperature of 145 K, where it begins to become obscured by the development of a second more weakly bound multilayer species γ. By 35 L, the β peak is merely a high temperature shoulder on the multilayer peak. β is assigned to the desorption of a bilayer, directly bound to the monolayer. The weaker bound multilayer species, γ, can be seen to appear from the broadening of the bilayer peak at an exposure of 15 L. This peak exhibits similar behavior to the bilayer peak with increasing coverage, i.e., increasing intensity coupled with an upward shift in peak temperature. This peak begins to dominate the spectrum at exposures >35 L and does not saturate up to exposures of 300 L, desorbing at a temperature of 152 K. Multilayer desorption is typically characterized by the sharing of leading edges of TPD traces, exhibiting zero-order desorption kinetics. Close inspection of the TPD traces in Fig. 5(c) show that this is not the case and, in fact, the desorption follows fractional-order kinetics. This is wholly consistent with the RAIRS data, where hydrogen bonded networks were evidenced by the characteristic broad nature of the υ(OH) stretching band. The presence of hydrogen bonding within the ethanol multilayer would lead to an expected deviation from perfect zero-order desorption kinetics in the TPD, as observed.

For exposures >50 L, a fourth peak begins to develop centered at ~155 K, labeled δ. With increasing exposure, this feature increases in intensity and broadens into a plateau centered around 157 K. One possible assignment for peak δ is to the desorption of monolayer ethanol since it has a similar desorption temperature to peak α, shown in Fig. 5(b). However, this possibility can be ruled out since the monolayer peak is found to saturate at an exposure ~10 L (see later).

Alternatively, peak δ can be assigned to the formation of crystalline ethanol within the multilayer as seen in the RAIRS experiments. The formation of crystalline ethanol is observed in the RAIR spectra (shown in Fig. 3) as a result of annealing between 120 and 140 K. In agreement with the appearance of peak δ in the TPD, crystalline ethanol is only observed in RAIRS for exposures $\geqslant$50 L. It is expected that crystalline ethanol would desorb at higher temperatures than the amorphous phase (peak γ), due to the larger number of hydrogen bonds that comprise the highly ordered crystalline structure. Furthermore, phase transitions within multilayer systems have been previously shown to lead to deformations in the TPD profile. The irreversible amorphous to crystalline phase transition for water is characterized by a distinctive bump on the leading edge of multilayer desorption.[45,46] Bolina *et al.* also attributed the appearance of a high temperature peak in the TPD of multilayer methanol adsorbed on

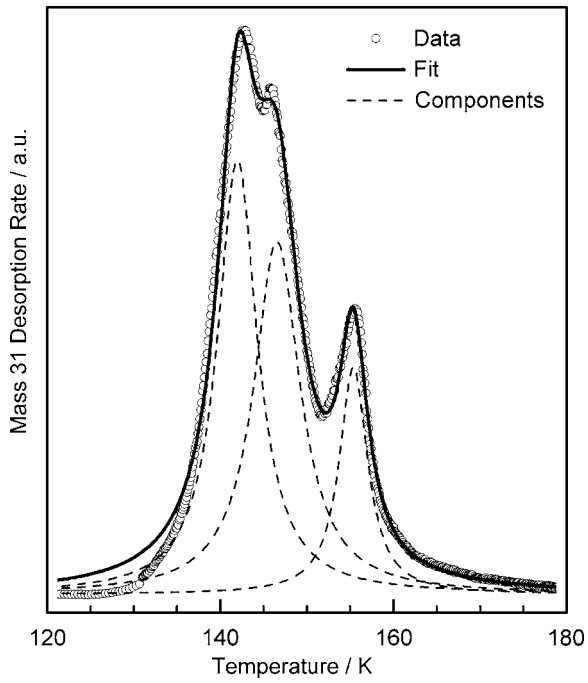

FIG. 6. Figure demonstrating the quality of the peak fitting procedure for an ethanol exposure of 25 L on HOPG at 98 K. The data (open circles) have been fitted with three separate Lorentzian peaks (dashed lines) corresponding to the number of desorption peaks observed in the TPD spectrum. The solid line represents the combined fit to the data.

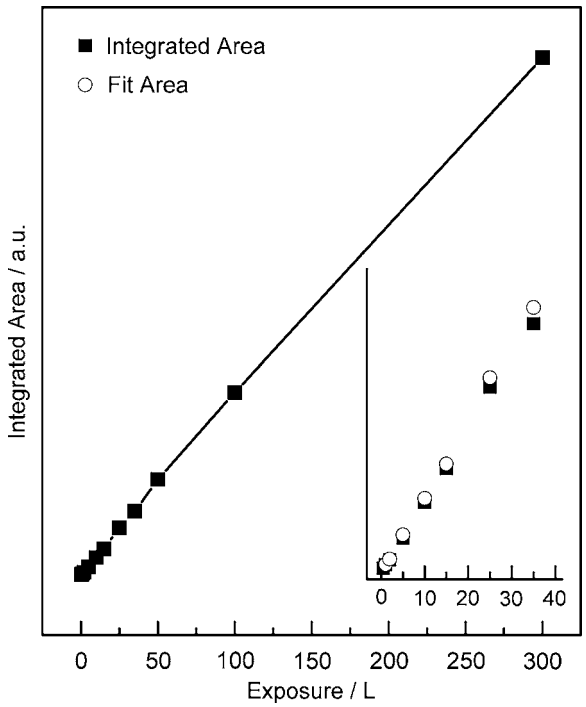

FIG. 7. A plot of the integrated area of the TPD traces, shown in Fig. 5, as a function of exposure. The inset shows a plot comparing the integrated areas of the TPD curves obtained from the raw data (squares) and those calculated from the fits (open circles).

HOPG to the formation of a crystalline species.[42] Therefore peak δ is most likely due to the formation of crystalline ethanol within the multilayer.

2. TPD analysis

Prior to conducting analysis of the data, each TPD trace was baseline corrected by fitting the residual background, then subtracting this from the original TPD data. It is clear from Fig. 5 that there is a significant degree of overlap between each of the desorbing species, α, β, and γ. Hence, to evaluate the contribution that each peak makes to the overall TPD trace necessitated curve fitting. Lorentzian line shapes provided the best overall fit to the data, yielding the best chi-squared value. Furthermore, the corresponding fitted peak temperatures and fitted areas compared well with the raw experimental data. The quality of the fitting is good up to a dose of 35 L, with an example shown in Fig. 6. However, for exposures in excess of 50 L, where the multilayer begins to dominate the spectrum and the crystalline form of ethanol develops in the monolayer region, curve fitting was unable to reproduce the accuracy obtained at the lower exposures. Curve fitting was only performed to allow the uptake of each individual ethanol species to be determined. The raw baseline corrected data, as seen in Fig. 5, were used for the determination of desorption orders and desorption energies.

Uptake curves. The uptake of ethanol as a function of exposure, determined by integrating the area under the TPD curves shown in Fig. 5, is plotted in Fig. 7. In our current experimental setup, it is not possible to measure the absolute coverage of ethanol on the surface. Hence, integration of the area under the TPD peak gives the relative coverage of the desorbing species. The linear increase over the entire exposure range in Fig. 7 indicates a constant sticking probability and is characteristic of precursor mediated adsorption. The data shown in Fig. 7 reaffirm the earlier observation that the variation in the uptake calculated for the RAIRS data (Fig. 2) is attributable to a change in molecular orientation rather than a change in sticking probability. Included as an inset to Fig. 7 is a plot showing the summation of the integrals from the fits and the raw data, highlighting the good quality of the fits to the TPD data.

Figure 8 shows the integrated areas of the individual desorption peaks α, β, and γ, as determined from the fitted TPD curves. The uptake of the α peak increases fairly linearly up to 10 L, achieving saturation around this exposure. The bilayer follows a similar trend, increasing fairly rapidly up to 20 L until saturation at ~25 L. Once the multilayer peak has appeared in the TPD spectrum at 15 L, the uptake of the γ feature exhibits a rapid increase with increasing exposure. The behavior of all three peaks reaffirms the peak assignments made on the basis of the TPD spectra shown in Fig. 5. The monolayer, α, and bilayer, β, exhibit saturation. In contrast, the multilayer, γ, does not saturate and is characterized by a constant increase with increasing exposure.

Bringing the observations from Fig. 5 and the data from Fig. 8 together, it is clear that subsequent ethanol adlayers form prior to saturation of the preceding layer. In the case of the bilayer, this is observed for an exposure of ~5 L. For multilayer growth, this is visible at a dose of ~15 L. Lee *et al.*[23] also observed the formation of an ethanol multilayer prior to saturation of the monolayer during X-ray photoelectron spectroscopy (XPS) measurements of ethanol adsorbed on Pt(111), noting a small contribution from the

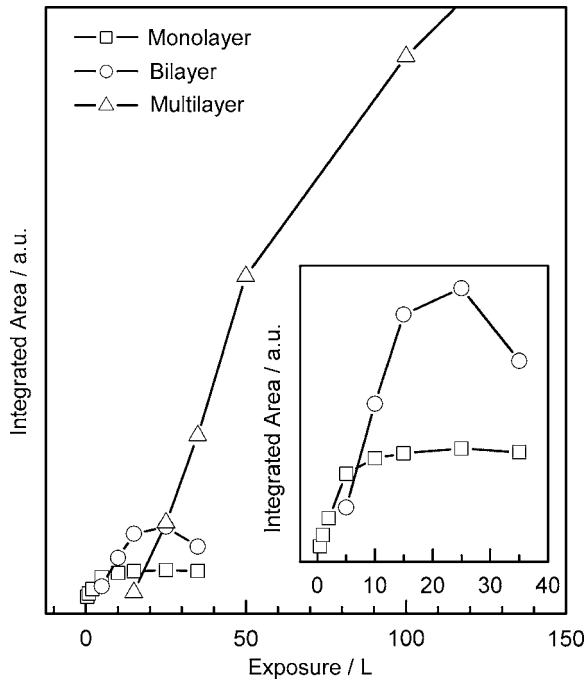

FIG. 8. Uptake curves for each separate desorption species determined by deconvolution of the experimental TPD traces seen in Fig. 5. The main plot shows the contributions from all three peaks: The monolayer (open squares), the bilayer (open circles), and the multilayer (open triangles). The inset shows monolayer and bilayer saturation on a larger scale. Note that the exposure range for the main plot is limited to 100 L to allow the saturation of monolayer and bilayer to be observed on a similar scale to the multilayer.

multilayer in the C 1*s* peak in XPS. Furthermore, similar behavior for methanol adsorbed on HOPG has also been reported.[42,47] These observations suggest that ethanol does not wet the HOPG surface but instead forms two-dimensional (2D) (monolayer) and three-dimensional (3D) (monolayer+bilayer) island clusters prior to forming a complete monolayer film.

Desorption orders. To gain further insight into the desorption of ethanol from the HOPG surface, quantitative analysis has also been performed on the TPD data. Such an approach yields information with regard to the desorption kinetics, i.e., the order of desorption, in addition to desorption energies and preexponential factors. A similar methodology has previously been applied to determine the desorption kinetics of methanol,[42] water,[45] and ammonia[48] adsorbed on HOPG at 97 K. The starting point of any TPD analysis is the Polanyi–Wigner equation[49,50]

$$r_{\mathrm{des}} = -\frac{d\theta}{dt} = \upsilon_n \theta^n \exp\left(\frac{-E_{\mathrm{des}}}{RT}\right), \tag{1}$$

where r_{des} is the rate of desorption, θ is the adsorbate coverage, υ_n is the desorption preexponential factor, n is the order of desorption, E_{des} is the desorption activation energy, R is the gas constant, T is the substrate temperature, and t is time. Recalling that the rate of change of coverage θ with time t [which is proportional to the signal intensity in the TPD trace $I(T)$] can be linked to the rate of change of coverage θ with temperature T (via the heating linear rate), Eq. (1) becomes

$$I(T) \propto \upsilon_n \theta^n \exp\left(\frac{-E_{\mathrm{des}}}{RT}\right). \tag{2}$$

Rearranging and taking logarithms, and remembering that only relative coverage θ_{rel} can be measured in our experiment, Eq. (2) becomes

$$\ln[I(T)] \propto \ln(\upsilon_n) + n \ln(\theta_{\mathrm{rel}}) - \frac{E_{\mathrm{des}}}{RT}. \tag{3}$$

Hence, plotting $\ln[I(T)]$ against $\ln[\theta_{\mathrm{rel}}]$ for a family of TPD curves at a fixed temperature yields a gradient which is equal to the desorption order n. Several assumptions have to be made in order to perform this plot. These include assuming that the preexponential factor and the energy of desorption do not vary significantly with coverage. However, these assumptions are likely to be valid in this case since ethanol is physisorbed on the HOPG surface.

Ideally, this calculation should be performed on a family of TPD curves consisting of a single desorption peak. It is clear from the TPD data in Fig. 5(a) that this can only be achieved for peak α. A plot of $\ln[I(T)]$ against $\ln[\theta_{\mathrm{rel}}]$ at a fixed temperature of $T=151$ K is shown in Fig. 9(a). The points used in the plot in Fig. 9(a) are taken from the leading edges of the TPD traces for exposures from 0.5 to 5 L, as indicated by the dotted line in Fig. 9(b). A similar calculation was performed for peak α for a range of different fixed temperatures and the results are summarized in Table II. It is clear from the data in Table II that the order of desorption for the monolayer does not depend on the value of the fixed temperature and remains relatively unchanged over the temperature range sampled. Peak α has an average desorption order of 0.98 ± 0.13 and hence follows first-order desorption kinetics. This result reaffirms the assignment of this peak to the monolayer.

Due to the high degree of overlap between the desorbing features obtained for ethanol exposures above 10 L, it is not possible to perform similar plots for peaks β and γ without contributions arising from the preceding peaks in the TPD spectrum. Therefore, plots using fixed temperatures in the range between 141 and 146 K show components from peaks α, β, and γ. Similar plots have been used previously to determine desorption orders for monolayer and multilayer methanol adsorbed on HOPG.[42]

Figure 9(c) shows a plot of $\ln[I(T)]$ against $\ln[\theta_{\mathrm{rel}}]$ at a fixed temperature of 141 K. The dotted line in Fig. 9(b) (low exposures) and Fig. 9(d) (high exposures) indicates the points on the TPD traces from which the plot was constructed. The plot exhibits three clearly defined gradients over the exposure range. This can be explained by reference to the TPD data [Figs. 5, 9(b), and 9(d)] and in regard to the selected temperature used to construct the plot. Each gradient in the plot corresponds to the most dominant peak in the TPD spectrum at the selected temperature. Hence, points obtained for exposures $\leqslant 2$ L pass through the leading edge of peak α and therefore give rise to a slope corresponding to the order of desorption for the monolayer. Similarly, points for exposures within the ranges from 5 to 15 L and from 25 to 300 L are dominated by contributions from peaks β (bilayer) and γ (multilayer), respectively, and hence yield

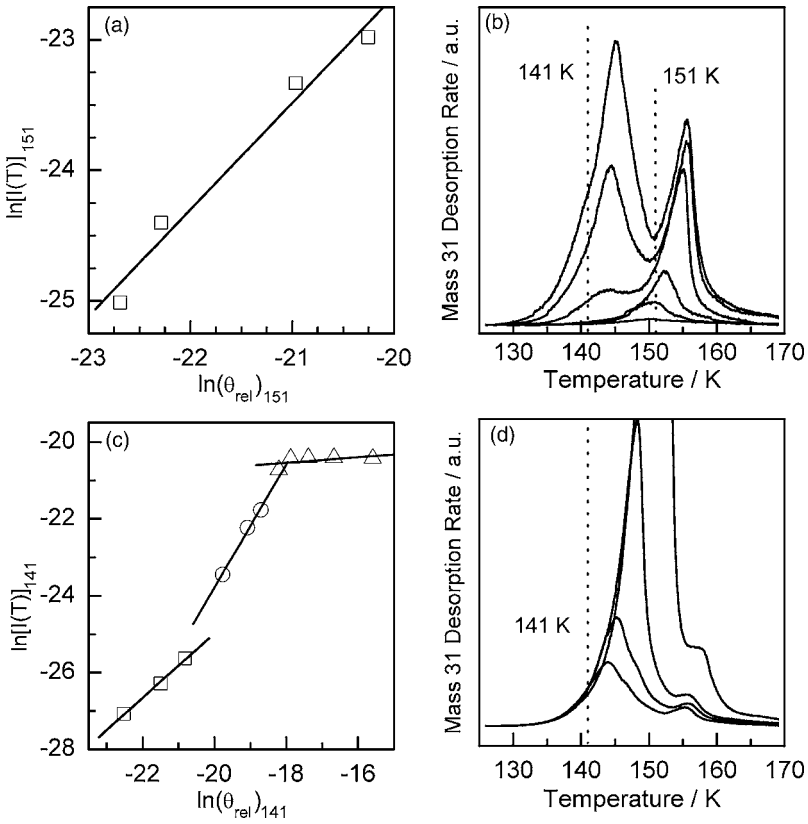

FIG. 9. (a) Graph of $\ln[I(T)]$ against $\ln(\theta_{rel})$ for a family of TPD curves at a fixed temperature of 151 K. The plot permits the determination of a desorption order of 0.98 ± 0.13 for the monolayer. The points for the plot in (a) are taken from the leading edges of the TPD traces for exposures between 0.5 and 5 L, as indicated by the dotted line on the TPD traces in (b). (c) shows a $\ln[I(T)]$ against $\ln(\theta_{rel})$ plot at a fixed temperature of 141 K and allows the determination of the desorption order for all three desorbing species. The three distinct gradients correspond to contributions from the monolayer (open squares), bilayer (open circles), and multilayer (open triangles) for exposures of 0.5–2, 5–15, and 25–300 L, respectively. The dotted line at 141 K in the TPD traces in (b) and (d) shows the points from which the plot is constructed at low and high exposures, respectively. Desorption orders of 1.52 ± 0.21 and 0.08 ± 0.07 were determined for the bilayer and multilayer, respectively.

slopes corresponding to desorption orders for these species. Desorption orders for all three peaks were calculated for a range of fixed temperatures in order to maximize the number of points for each peak. The data from these calculations are summarized in Table II.

As already seen for peak α, the data in Table II show that the desorption orders for peaks β and γ are relatively constant, irrespective of the temperature chosen to perform the order plot. Furthermore, the desorption orders for peak α obtained from plots consisting of three separate contributions [Fig. 9(c)] are consistent with those obtained for plots where peak α is the only peak used in the calculation [Fig. 9(a)]. Table II shows that peak β has a calculated desorption order of 1.52 ± 0.21. This value, well in excess of first-order desorption, implies a cooperative effect between the ethanol molecules during desorption. Calculated desorption orders for peak γ are 0.08 ± 0.07 and show that the multilayer follows fractional-order desorption. Fractional-order kinetics are consistent with the TPD spectra [Fig. 5(c)], which do not share leading edges, as expected for perfect zero-order desorption. Fractional-order desorption for the multilayer is ascribed to hydrogen bonding within the multilayer. This is supported by the RAIRS data (Fig. 1) that exhibits a broad υ(OH) stretching band at 3280 cm^{-1}, which is a distinctive feature of hydrogen bonding. Fractional-order desorption, which has been assigned to the presence of hydrogen bonding, has also been observed for multilayer H_2O (Ref. 45) and methanol[42] ices adsorbed on HOPG.

TABLE II. Table showing the calculated desorption orders for monolayer (peak α), bilayer (peak β), and multilayer (peak γ) ethanol adsorbed on HOPG at 98 K.

Temperature (K)	Desorption order n		
	Peak α	Peak β	Peak γ
156	0.98		
155	0.92		
154.5	0.91		
151	0.85		
146	0.99	1.50	0.10
145	1.21	1.32	0.09
142	0.89	1.74	0.08
141	1.05	1.66	0.07

Desorption energies. Using the calculated desorption orders, the energy of desorption can be obtained by further rearrangement of Eq. (3)

$$\ln[I(T)] - n \ln \theta_{rel} \propto \ln \upsilon_n - \frac{E_{des}}{RT}. \quad (4)$$

Hence, for a single TPD spectrum, plotting $\ln[I(T)]$-$n \ln(\theta_{rel})$ against $1/T$ will yield a plot with a straight line of gradient $-E_{des}/R$ for the correct order of desorption. The average value of the desorption energy E_{des} can then be obtained. Again, this calculation assumes a constant preexponential factor (as a function of coverage), which is a reasonable assumption since ethanol is physisorbed on HOPG at all exposures at 98 K.

An attempt was made to calculate desorption energies for all three species adsorbed on the HOPG surface. However, values obtained for the monolayer led to inconsistent results. Figure 5 clearly shows that there is a significant degree of overlap between all three desorbing species. This

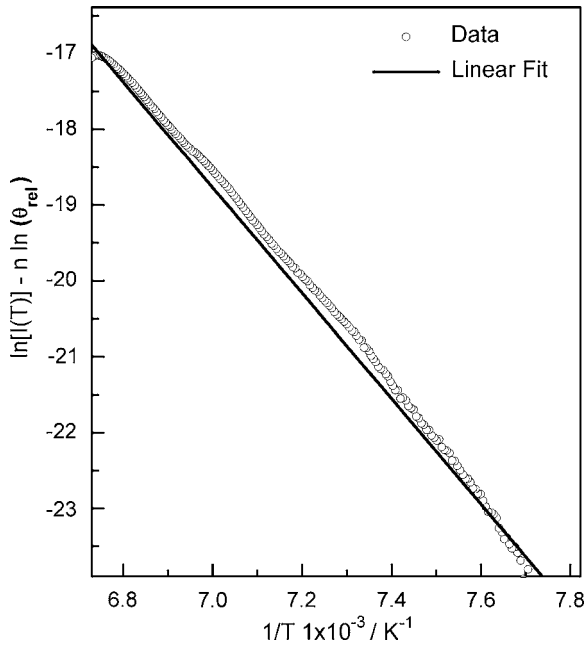

FIG. 10. Graph of $\ln[I(T)]-n\ln(\theta_{\mathrm{rel}})$ against $1/T$ for multilayer ethanol following an exposure of 100 L on HOPG at 98 K. The data are plotted with a desorption order of $n=0.08$. The average desorption energy of 56.3 ± 1.7 kJ mol^{-1} is calculated from the gradient $-E_{\mathrm{des}}/R$.

overlap is particularly prominent between ethanol exposures of 5 and 25 L, i.e., when the bilayer and multilayer begin to appear in the TPD spectrum. The leading edge of the TPD trace that is required to determine desorption energies for the monolayer[51] falls into this exposure range. A consequence of this overlapping behavior is a reduction in the number of TPD traces that can be used to accurately determine the desorption energy values. The very low dose (0.5–2 L) TPD traces that exhibited a single peak contain an insufficient number of data points to generate reliable results and, therefore, the calculation of desorption energies for the monolayer is heavily reliant on curve fitting. Since curve fitting does not accurately reproduce the leading edge of the TPD spectra (Fig. 6), desorption energies have only been calculated for the multilayer (peak γ) and bilayer (peak β), where the leading edges could be confidently assigned without the need for curve fitting.

Figure 10 shows a plot of $\ln[I(T)]-n\ln(\theta_{\mathrm{rel}})$ against $1/T$ for an exposure of 100 L. The quality of the linear fit to the data is excellent (typically giving R^2 values of 0.999) and is representative of all multilayer exposures above 35 L. At these exposures, the leading edge can be confidently assigned to the multilayer species. An average desorption energy of 56.3 ± 1.7 kJ mol^{-1} has been determined for the multilayer and is consistent over the range sampled (Table III). The errors in the desorption energies listed in Table III are calculated using the variation in the desorption order of the multilayer.

Desorption energy calculations for the bilayer were performed on TPD spectra where the leading edge of the TPD profile was not obscured by the formation of the multilayer. These measurements were therefore limited to exposures between 5 and 15 L and yielded an average desorption energy of 53.3 ± 3.1 kJ mol^{-1}. The values are consistent over the exposure range and are also summarized in Table III. Within experimental error, desorption energies for the bilayer are in close agreement with those obtained for the multilayer, which is to be expected considering the similarity in desorption temperature between the two species.

TABLE III. Table showing the desorption energies of multilayer ethanol on HOPG at 98 K. The orders of desorption used in the calculations were $n=0.08$ and $n=1.52$ for the multilayer and bilayer, respectively. Errors are determined using the variation in the desorption order n.

Multilayer		Bilayer	
Exposure (L)	Desorption energy (kJ mol^{-1})	Exposure (L)	Desorption energy (kJ mol^{-1})
35	56.0 ± 1.1		
50	55.2 ± 1.3	5	50.1 ± 2.4
100	56.8 ± 1.0	10	55.8 ± 0.8
300	57.8 ± 1.9	15	53.2 ± 3.0

The value of the multilayer desorption energy determined here is slightly higher when compared to those reported previously for ethanol desorption from HOPG of 46 ± 3 kJ (Ref. 32) and 46.4 ± 0.8 kJ mol^{-1}.[31] The higher energy for multilayer desorption determined in this work may be explained by the differing film thicknesses investigated here compared to those of Shukla *et al.*[31] and Ulbricht *et al.*[32] Our ethanol films correspond to a thickness of ~10 ML following a 300 L exposure, whereas Ulbricht *et al.*[32] reported desorption energies for 4 ML thick films. As seen in Fig. 5(b), it is likely that 4 ML thick films are comprised of the monolayer and bilayer species. Hence, previously reported desorption energies for multilayer ethanol desorption may actually arise from bilayer ethanol rather than the multilayer. The desorption energy of the bilayer is ~3 kJ mol^{-1} lower than the multilayer and therefore our bilayer desorption energies (although still a little high) are in much closer agreement with the values previously reported.[31,32]

Preexponential factor. The preexponential factor for the multilayer can be determined from the order of desorption and desorption energy as calculated above. For the data reported here, it is not possible to calculate the preexponential factor from an Arrhenius plot since the absolute coverage of ethanol on the surface is not known. However, the preexponential factor can be estimated by conversion of the experimentally measured relative intensity and relative coverage into actual intensity and actual coverage. This can be achieved by estimating the exposure for monolayer saturation. It is then possible to determine the approximate number of adsorbates that correspond to monolayer coverage. Using the fact that the sticking probability of ethanol is constant over all exposures (Fig. 7), it is then possible to scale the relative coverage to absolute coverage.

The surface atom density of the HOPG surface has been determined previously[45] to be 3.82×10^{19} atoms m^{-2}. In order to calculate the number of molecules adsorbed on the surface and hence determine an estimate of the absolute coverage, a few approximations need to be made. Figure 8 indicates that monolayer saturation is achieved following an ethanol exposure of 10 L. The value for the number of ethanol

molecules per unit area has been taken from Morishige,[33] who estimated a monolayer capacity of ethanol adsorbed on Grafoil at 30 K to be 4.92×10^{18} molecules m^{-2}. The actual coverage for 10 L ethanol exposure is given by the number of ethanol molecules per unit area divided by the atom density of the HOPG surface and is therefore ~0.13 ML.

The total uptake of ethanol on the HOPG surface is constant as a function of exposure (Fig. 7). Therefore, the number of adsorbates can be directly related to the area under the TPD curves shown in Fig. 5. Consequently, a scaling factor can be derived from this relation in order to convert all mass spectrometer intensities into absolute intensities and hence the relative coverage can be converted to an absolute coverage. The TPD data shown in Fig. 5 clearly show that the bilayer provides a significant contribution to the integrated area under the curve at an exposure of 10 L. Hence, to obtain an accurate scaling factor, the relative coverage is calculated from the integrated area obtained from the fit to the monolayer and not from the total area under the raw data TPD profile. The area under the fit for the monolayer is 2.2×10^{-9} a.u., which in turn corresponds to an absolute coverage of 4.92×10^{18} molecules m^{-2}. Hence, a scaling factor of 2.3×10^{27} has been used to convert relative coverage to absolute coverage values.

To calculate the preexponential factor for multilayer desorption requires rearrangement of Eq. (1)

$$\upsilon_n = \frac{I(T)}{\theta^n \exp\left[\frac{-E_{\mathrm{des}}}{RT}\right]}, \tag{5}$$

where $I(T)$ is the mass spectrometer scaled intensity, θ is the actual coverage derived from $I(T)$, and n and E_{des} are the calculated values for the desorption order and desorption energy, respectively. Using Eq. (5), an average value of the preexponential factor was determined for each TPD spectrum for all exposures above 35 L. These values exhibited no exposure dependence, thus reaffirming the earlier assumption that the preexponential factor does not vary with coverage.

The average value for the preexponential factor obtained for multilayer desorption of ethanol from HOPG is $2.2\times10^{37\pm2}$ molecules m^{-2} s^{-1}. Typically, preexponential factors for multilayer desorption are expected to be of the order $\sim10^{26}$ molecules m^{-2} s^{-1},[52] hence, the value reported here might be considered to be high. Since several assumptions were made in obtaining this value, various tests were performed in order to check the validity of the assumptions made in the calculation. The estimated monolayer saturation, assumed to occur at 10 L (corresponding to a coverage of 0.13 ML), was verified by performing additional calculations. The 0.13 ML coverage was assumed to be formed for a variety of exposures, ranging from a lower limit of 5 L to an upper limit of 20 L. The preexponential factor proved to be insensitive to the value of saturation coverage, yielding an error well within the error range quoted above. Errors associated with the desorption order and desorption energy were also propagated through the calculation. Incorporating the spread of values obtained from these parameters into Eq. (5) demonstrated that the value of the preexponential factor exhibits the most dependence on the value of the desorption order. Errors associated with the variation of desorption order were an order of magnitude greater than those obtained from using the variation of desorption energy. Similar conclusions were drawn from calculations using the same methodology to determine the preexponential factor for multilayer desorption of H_2O from HOPG.[45]

IV. CONCLUSIONS

A detailed RAIRS and TPD study of ethanol adsorbed on the HOPG surface at 98 K has been performed. RAIRS shows that ethanol adsorbs reversibly on the HOPG surface, forming physisorbed multilayers at all exposures. Annealing the multilayer ices at ethanol exposures $\geqslant$50 L shows the formation of crystalline ethanol, characterized by sharpening of the υ(OH) band and splitting of the υ(CO) and υ(CC) bands. TPD measurements show four distinct species adsorbed on the HOPG surface. Two saturated species are formed: a monolayer, which is directly associated with the HOPG surface, and a bilayer. Higher exposures show the growth of multilayer ethanol, which dominates the TPD spectra for doses above 50 L. At the highest exposures, crystalline ethanol is also observed.

As expected, hydrogen bonding plays a significant role in ethanol adsorption on the HOPG surface. Low ethanol exposures give rise to the formation of 2D (monolayer) and 3D clusters (bilayer growth) on the substrate prior to the formation of the multilayer. RAIRS data exhibit a broad υ(OH) band in the spectrum at 3280 cm^{-1}, which is characteristic of hydrogen bonding. Furthermore, the multilayer is shown to desorb with fractional-order kinetics, which is also ascribed to the presence of hydrogen bonding. TPD data have been used to calculate the desorption energy and preexponential factor for multilayer desorption. Values of 56.3 ± 1.7 kJ mol^{-1} for the desorption energy and $2.2\times10^{37\pm2}$ molecules m^{-2} s^{-1} for the preexponential factor have been determined.

The study undertaken here provides detailed information on the desorption of ethanol adsorbed on dust grain surfaces that is relevant to the chemistry of hot cores. Thermal desorption of interstellar ices from grain surfaces plays a key role in the chemistry observed in star forming regions. The heat generated by new born stars leads to the evaporation of chemically rich icy mantles, yielding gas-phase abundances of numerous simple molecules that are well in excess of those predicted by gas-phase models. Recent studies have shown that the thermal desorption of these ices is not an instantaneous process as previously thought.[35] Hence, kinetic parameters that accurately describe thermal desorption of astrophysically relevant molecules adsorbed on dust grains are essential for the accurate modeling of star forming processes.

ACKNOWLEDGMENTS

The U.K. EPSRC is gratefully acknowledged for Ph.D. studentships for A.J.W. and J.L.E. in addition to an equipment and consumables grant (GR/S 15273/01). The Leverhulme trust is thanked for a postdoctoral fellowship for D.J.B. This work forms part of the research currently being

undertaken in the UCL Centre for Cosmic Chemistry and Physics.

[1] T. J. Millar, G. H. Macdonald, and R. J. Habing, Mon. Not. R. Astron. Soc. **273**, 25 (1995).
[2] T. J. Millar, H. Olofsson, A. Hjalmarson, and P. D. Brown, Astron. Astrophys. **205**, L5 (1988).
[3] M. Ohishi, I.-S. Ishikawa, S. Yamamoto, S. Saito, and T. Amano, Astrophys. J. **446**, L43 (1995).
[4] B. E. Turner, Astrophys. J., Suppl. Ser. **76**, 617 (1991).
[5] E. Herbst and C. M. Leung, Astrophys. J., Suppl. Ser. **69**, 271 (1989).
[6] T. J. Millar, E. Herbst, and S. B. Charnley, Astrophys. J., Suppl. Ser. **369**, 147 (1991).
[7] P. D. Brown, S. B. Charnley, and T. J. Millar, Mon. Not. R. Astron. Soc. **231**, 409 (1988).
[8] S. B. Charnley, M. E. Kress, A. Tielens, and T. J. Millar, Astrophys. J. **448**, 232 (1995).
[9] W. W. Duley and D. A. Williams, *Interstellar Chemistry* (Academic, New York, 1984).
[10] L. J. Allamandola, M. P. Bernstein, S. A. Sandford, and R. L. Walker, Space Sci. Rev. **90**, 219 (1999).
[11] N. Boudin, W. A. Schutte, and J. M. Greenberg, Astron. Astrophys. **331**, 749 (1998).
[12] T. I. Hasegawa, E. Herbst, and C. M. Leung, Astrophys. J., Suppl. Ser. **82**, 167 (1992).
[13] A. Shriver, L. Schriver-Mazzuoli, P. Ehrenfreund, and L. d'Hendecourt, Chem. Phys. **334**, 128 (2007).
[14] J. P. Perchard and M. L. Josien, J. Chim. Phys. Phys.-Chim. Biol. **65**, 1856 (1968).
[15] J. P. Perchard and M. L. Josien, J. Chim. Phys. Phys.-Chim. Biol. **65**, 1834 (1968).
[16] Y. Mikawa, J. W. Brasch, and R. J. Jakobsen, Spectrochim. Acta, Part A **27**, 529 (1971).
[17] A. J. Barnes and H. E. Hallam, Trans. Faraday Soc. **66**, 1932 (1970).
[18] S. Coussan, Y. Bouteiller, J. P. Perchard, and W. Q. Zheng, J. Phys. Chem. A **102**, 5789 (1998).
[19] J. P. Camplin and E. M. McCash, Surf. Sci. **360**, 229 (1996).
[20] H. Dothe, M. A. Lowe, and J. S. Alper, J. Phys. Chem. **93**, 6632 (1989).
[21] J. Eng, K. Raghavachari, L. M. Struck, Y. J. Chabal, B. E. Bent, G. W. Flynn, S. B. Christman, E. E. Chaban, G. P. Williams, K. Radermacher, and S. Manti, J. Chem. Phys. **106**, 9889 (1997).
[22] C. Panja, N. Saliba, and B. E. Koel, Surf. Sci. **395**, 248 (1998).
[23] A. F. Lee, D. E. Gawthrope, N. J. Hart, and K. Wilson, Surf. Sci. **548**, 200 (2004).
[24] B. A. Sexton, K. D. Rendulic, and A. E. Hughes, Surf. Sci. **121**, 181 (1982).
[25] M. Bowker and R. J. Madix, Surf. Sci. **116**, 549 (1982).
[26] D. C. Papageorgopoulos, Q. Ge, and D. A. King, J. Phys. Chem. **99**, 17645 (1995).
[27] E. Vesselli, A. Baraldi, G. Comelli, S. Lizzit, and R. Rosei, ChemPhysChem **5**, 1133 (2004).
[28] R. Shekhar and M. A. Barteau, Catal. Lett. **31**, 221 (1995).
[29] J. Z. Xu, X. P. Zhang, R. Zenobi, J. Yoshinobu, Z. Xu, and J. T. Yates, Surf. Sci. **256**, 288 (1991).
[30] C. J. Weststrate, W. Ludwig, J. W. Bakker, A. C. Gluhoi, and B. E. Nieuwenhuys, ChemPhysChem **8**, 932 (2007).
[31] N. Shukla, J. Gui, and A. J. Gellman, Langmuir **17**, 2395 (2001).
[32] H. Ulbricht, R. Zacharia, N. Cindir, and T. Hertel, Carbon **44**, 2931 (2006).
[33] K. Morishige, J. Chem. Phys. **97**, 2084 (1992).
[34] K. W. Herwig and F. R. Trouw, Phys. Rev. Lett. **69**, 89 (1992).
[35] S. Viti and D. A. Williams, Mon. Not. R. Astron. Soc. **305**, 755 (1999).
[36] S. Viti, M. P. Collings, J. W. Dever, M. R. S. McCoustra, and D. A. Williams, Mon. Not. R. Astron. Soc. **354**, 1141 (2004).
[37] D. A. Williams, Faraday Discuss. **109**, 1 (1998).
[38] W. A. Brown, S. Viti, A. J. Wolff, and A. S. Bolina, Faraday Discuss. **133**, 113 (2006).
[39] R. Wiesendanger, L. Eng, H. R. Hidber, P. Oelhafen, L. Rosenthaler, U. Staufer, and H. J. Guntherodt, Surf. Sci. **189**, 24 (1987).
[40] O. Haida, H. Suga, and S. Seki, J. Chem. Thermodyn. **9**, 1133 (1977).
[41] J. Heidberg and M. Warskulat, J. Electron Spectrosc. Relat. Phenom. **54/55**, 961 (1990).
[42] A. S. Bolina, A. J. Wolff, and W. A. Brown, J. Chem. Phys. **122**, 044713 (2005).
[43] R. Souda, J. Chem. Phys. **122**, 134711 (2005).
[44] P. Ayotte, R. S. Smith, G. Teeter, Z. Dohnalek, G. A. Kimmel, and B. D. Kay, Phys. Rev. Lett. **88**, 245505 (2002).
[45] A. S. Bolina, A. J. Wolff, and W. A. Brown, J. Phys. Chem. B **109**, 16836 (2005).
[46] Z. Dohnalek, R. L. Ciollo, G. A. Kimmel, K. P. Stevenson, R. S. Smith, and B. D. Kay, J. Chem. Phys. **110**, 5489 (1999).
[47] L. Wang, Y. H. Song, A. G. Wu, Z. Li, B. L. Zhang, and E. K. Wang, Appl. Surf. Sci. **199**, 67 (2002).
[48] A. S. Bolina and W. A. Brown, Surf. Sci. **598**, 45 (2005).
[49] A. M. de Jong and J. W. Niemantsverdriet, Surf. Sci. **233**, 355 (1990).
[50] D. A. King, Surf. Sci. **47**, 384 (1975).
[51] C. Pisani, G. Rabino, and F. Ricca, Surf. Sci. **41**, 277 (1974).
[52] W. A. Brown and A. S. Bolina, Mon. Not. R. Astron. Soc. **374**, 1006 (2007).